0.01 mM thiamine, 0.004% each of 18 amino acids (the standard ones minus Cys and Met), 0.005% L-(+)-selenomethionine and 30 mg of ampicillin. The seed culture, grown at 30 °C overnight in Luria broth (20 ml), was centrifuged and the pellets added to the culture medium. The mixture was incubated at 36 °C for 16 h with orbital shaking. The bacterial suspension was centrifuged at 12,000*g* at 0 °C for 8 min. The pellets and the supernatant contained 18 mg and 3 mg of apoaequorin, respectively. The apoaequorin in the pellets was extracted, regenerated into aequorin and purified as described[8] to yield 14 mg of pure selenomethionine-substituted aequorin. The selenium content of the protein determined by electrospray ionization mass spectrometry indicated that more than 90% of the five methionine residues were substituted.

Crystallization

Crystals were grown at 17 °C by hanging droplet vapour diffusion. Drops consisted of 3 µl of 10 mg ml^{-1} protein in 2 mM EDTA, 1.2 M ammonium sulphate, 10 mM Bis-Tris pH 7.2 with an equal volume of the well liquor, 63% saturated ammonium sulphate, 10 mM Bis-Tris pH 7.2. Crystals took a week to appear and up to two months to grow to a size suitable for diffraction. The crystals grow as square sectioned rods, the native recombinant protein reaching dimensions of 0.6 × 0.1 × 0.1 mm, the selenomethionyl protein growing no bigger than 0.3 × 0.07 × 0.07 mm.

Data collection

Data were collected at the Brookhaven National Synchrotron Light Source, beamline X8-C. Crystals were cryoprotected by adding glycerol to mother liquor to 15% (v/v). Crystals were flash frozen in the nitrogen stream of an Oxford Cryosystem before data collection. Crystals of native aequorin diffracted to 2.3 Å, whereas smaller selenomethionine-containing crystals diffracted to only 3.5 Å. All data were processed and reduced using DENZO and SCALEPACK[23]. The space group of crystals of both protein forms was determined to be $P4_32_12$. Unit-cell dimensions for the native protein were $a = b = 81.27$ Å, $c = 163.66$ Å, for the selenomethionyl protein $a = b = 81.98$ Å, $c = 164.32$ Å. Data were collected on the selenium-containing crystal at three wavelengths to enable MAD phasing (Table 2).

Phasing

Phases were determined from the MAD data using the program SOLVE[24]. This gave 10 selenium sites, consistent with 2 molecules in the asymmetric unit, 5 sites in each molecule. Initial electron density maps indicated α-helices and molecular boundaries. The phased selenium data were then subjected to density modification using the program DM[25], including twofold NCS averaging. Maps obtained from the DM-modified data showed clear electron density for most of the chain of each molecule, including significant side-chain density. On the basis of these maps and the known location of the selenium atom sites, the chain was readily traced from residues 3 to 189 using the program O[26].

Refinement

The initial model was refined against the selenium data (peak wavelength) with strict NCS constraints using CNS[27] including simulated annealing to 4,000 K. After some rebuilding, this model was subsequently refined using native data, with phases gradually extended using DM to 2.3 Å. To this point, the refined model contained no coelenterazine. Tautomeric models of coelenterazine were built and minimized. An excellent fit to density was obtained using the model based on the tautomer shown in Fig. 3 with a tetragonal, sp^3, carbon at the C2 position. The exception to the good fit was an unoccupied extension of the density from the position of the C2 atom, strongly emphasized in $F_o - F_c$ maps. This density could be readily fit by a hydroperoxide bonded at C2, as previously suggested[3,12]. The ligand was therefore rebuilt with the peroxide and used for subsequent modelling. Parameter and topology files for refinement of the peroxidized coelenterazine were obtained using the Hetero Compound Information Centre[28]. The whole structure was then further refined, including restrained NCS, and water molecules added (Table 2).

As electron density for the peroxide group in the refined model appeared weaker than the rest of the coelenterazine, the peroxide atoms were subjected to occupancy refinement. This showed ~60% occupancy of this part of the ligand in molecule A and ~55% in molecule B. Measurement of light emission from redissolved aequorin crystals shows that when the crystals are obtained from the mother liquor they retain ~90% of the light-emitting capacity of the native protein; however, after X-ray irradiation crystals show less than 50% activity. This is consistent with loss of the peroxide during the data collection as the result of radiation damage.

Received 16 December 1999; accepted 20 March 2000.

1. Shimomura, O., Johnson, F. H. & Saiga, Y. Extraction, purification and properties of aequorin, a bioluminescent protein from the luminous hydromedusan, *Aequorea*. *J. Cell. Comp. Physiol.* **59,** 223–240 (1962).
2. Inouye, S. *et al.* Cloning and sequence analysis of cDNA for the luminescent protein aequorin. *Proc. Natl Acad. Sci.* **82,** 3145–3158 (1985).
3. Shimomura, O. & Johnson, F. H. Peroxidized coelenterazine, the active group in the photoprotein aequorin. *Proc. Natl Acad. Sci. USA* **75,** 2611–2615 (1978).
4. Shimomura, O. & Johnson, F. H. Chemical nature of light emitter in bioluminescence of aequorin. *Tetrahedron Lett.* **31,** 2963–2966 (1973).
5. Shimomura, O. & Johnson, F. H. Regeneration of the photoprotein aequorin. *Nature* **256,** 236–238 (1975).
6. Prasher, D., McCann, R. O. & Cormier, M. J. Cloning and expression of the cDNA coding for aequorin, a bioluminescent calcium-binding protein. *Biochem. Biophys. Res. Commun.* **126,** 1259–1263 (1985).
7. Hannick, L. I., Prasher, D. C., Schultz, L. W., Deschamps, J. R. & Ward, K. B. Preparation and initial characterization of crystals of the photoprotein aequorin from *Aequorea victoria*. *Proteins Struct. Funct. Genet.* **15,** 103–107 (1993).
8. Shimomura, O. & Inouye, S. The *in situ* regeneration and extraction of recombinant aequorin from *Escherichia coli* cells and the purification of extracted aequorin. *Protein Expr. Purif.* **16,** 91–95 (1999).
9. Tanaka, T., Ames, J. B., Harvey, T. S., Stryer, L. & Ikura, M. Sequestration of the membrane-targeting myristoyl group of recoverin in the calcium-free state. *Nature* **376,** 444–447 (1995).
10. Vijay-Kumar, S. & Cook, W. J. Structure of a sarcoplasmic calcium-binding protein from Nereis diversicolor refined at 2. 0 A resolution. *J. Mol. Biol.* **224,** 413–426 (1992).
11. Cook, W. J., Jeffrey, L. C., Cox, J. A. & Vijay-Kumar, S. Structure of a sarcoplasmic calcium-binding protein from amphioxus refined at 2. 4 Ångstroms resolution. *J. Mol. Biol.* **229,** 461–471 (1993).
12. Musicki, B., Kishi, Y. & Shimomura, O. Structure of functional part of photoprotein aequorin. *J. Chem. Soc. Chem. Commun.* **126,** 1256–1268 (1986).
13. Ohmiya, Y. & Tsuji, F. I. Bioluminescence of the Ca^{2+}-binding photoprotein, aequorin, after histidine modification. *FEBS Lett.* **320,** 267–270 (1993).
14. Ohmiya, Y., Ohashi, M. & Tsuji, F. I. Two excited states in aequorin bioluminescence induced by tryptophan modification. *FEBS Lett.* **301,** 197–201 (1992).
15. Tsuji, F. I., Inouye, S., Goto, T. & Sakaki, Y. Site-specific mutagenesis of the calcium-binding photoprotein aequorin. *Proc. Natl Acad. Sci.* **83,** 8107–8111 (1986).
16. Shimomura, O., Musicki, B. & Kishi, Y. Semi-synthetic aequorin. An improved tool for the measurement of calcium ion concentration. *Biochem. J.* **251,** 405–410 (1988).
17. Shimomura, O., Musicki, B. & Kishi, Y. Semi-synthetic aequorins with improved sensitivity to Ca^{2+} ions. *Biochem. J.* **261,** 913–920 (1989).
18. Shimomura, O., Inouye, S., Musicki, B. & Kishi, Y. Recombinant aequorin and recombinant semi-synthetic aequorins. Cellular Ca^{2+} ion indicators. *Biochem. J.* **270,** 309–312 (1990).
19. Shimomura, O. Luminescence of aequorin is triggered by the binding of two calcium ions. *Biochem. Biophys. Res. Commun.* **211,** 359–363 (1995).
20. Shimomura, O. & Inouye, S. Titration of recombinant aequorin with calcium chloride. *Biochem. Biophys. Res. Commun.* **221,** 77–81 (1996).
21. Nomura, M., Inouye, S., Ohmiya, Y. & Tsuji, F. I. A C-terminal proline is required for bioluminescence of the Ca^{2+}-binding photoprotein, aequorin. *FEBS Lett.* **295,** 63–66 (1991).
22. Inouye, S., Aoyama, S., Miyata, T., Tsuji, F. I. & Sakaki, Y. Overexpression and purification of the recombinant Ca^{2+}-binding protein, apoaequorin. *J. Biochem. (Tokyo)* **105,** 473–477 (1989).
23. Otwinowski, Z. in *Proceedings of the CCP4 Study Weekend: Data Collection and Processing.* (eds Sawyers, L. Isaacs, N. & Bailey, S.) 56–62 (SERC Daresbury Laboratory, Warrington, UK; 1993).
24. Terwilliger, T. C. & Berendzen, J. Automated structure solution for MIR and MAD. *Acta Crystallogr. D* **55,** 849–861 (1999).
25. Collaborative Computational Project No. 4. The CCP4 suite: programs for protein crystallography. *Acta Crystallogr. D* **50,** 760–763 (1994).
26. Jones, T. A., Zou, J. Y., Cowan, S. W. & Kjeldgaard, M. Improved methods for building protein models in electron density maps and the location of errors in these models. *Acta Crystallogr. A* 47, 110–119 (1991).
27. Brunger, A. T. *et al.* Crystallography & NMR system: A new software suite for macromolecular structure determination. *Acta Crystallogr. D* **54,** 905–921 (1998).
28. Kleywegt, G. J. & Jones, T. A. Databases in protein crystallography. *Acta Crystallogr. D* **54,** 1119–1131 (1998).
29. Guex, N. & Peitsch, M. C. SWISS-MODEL and the Swiss-PdbViewer: An environment for comparative protein modeling. *Electrophoresis* **18,** 2714–2723 (1997).
30. POVRAY. Persistence of Vision Raytracer version 3. 1. ⟨http://www.povray.org⟩

Acknowledgements

We thank B. Kaminer for initiating this collaborative effort; B. Seaton for involvement in early crystallization studies; H. Nakamura for structural information on imidazopyrazinone; and the Boston University Mass Spectrometry Facility. This work was supported in part by NSF grants to O.S. and to J.F.H.

Correspondence and requests for materials should be addressed to J.F.H. (e-mail: jfh@medxtal.bu.edu). The coordinates of the structure have been deposited in the Protein Data Bank under accession code 1EJ3.

erratum

The ecological cost of sex

C. Patrick Doncaster, Graeme E. Pound & Simon J. Cox

Nature **404,** 281–285 (2000)

In Fig. 2a, the right-hand label on the horizontal axis should have read

$$\frac{k_2}{\alpha_{21}}$$

and the axis label on the horizontal axis should have been 'Abundance of Predator-1 (N_1)'. □

germinating cohorts were followed for arcs established in 1997. Individuals established before the beginning of the study ('older') were included in the census. Thus, there were a total of 6 older cohorts and 12 germinating cohorts (3 from 1996, 6 from 1997 and 3 from 1998).

Censuses were conducted in May and September of 1996, 1997 and 1998. Seedlings' distance to parent and distance to all other seedlings were calculated using x, y coordinates. Neighbourhood density was estimated by the number of conspecific seedlings/saplings within a 20 cm radius. Neighbourhood density for individuals along the arc's edge was adjusted by projecting a mirror image of seedling distribution 20 cm within the arc.

Separating distance and density effects

In logistic regression models, distance to parent and neighbourhood density were entered as independent variables, and seedling status (alive or dead) was entered as the dependent variable. Density at germination was used for seedlings, whereas density at the first census was used for older individuals. Logistic regression analyses were conducted using SPSS, version 6.1.3. Comparisons of mean distance to parent at initial and subsequent census dates were made by generating reliability estimates using Resampling Stats, version 3.14.

Effect of soil

Fruits were collected from three trees in Bloomington with large crops. Fruit flesh was removed, and seeds were surface sterilized (1 min 70% alcohol, 3 min 50% bleach, 1 min 70% alcohol, 1 min distilled water). To break dormancy, seeds were stratified in wet sterile sand at 4 °C for 5–6 months. Soil was collected at distances of 0–5 m and 25–30 m beneath trees 1, 4 and 6. Soil was sieved and root material was cut into ~1 cm pieces and returned to the soil. Soil samples were diluted 1 : 1 v/v with sterile potting mix (Metro Mix). One half of the soil in each distance class was autoclaved for 4 h at 211 °C. Seedlings that germinated following stratification were planted in each of four soil types (near/far, sterile/unsterile) and watered individually to prevent cross-contamination. Growth and survival of seedlings were monitored for 2 months in the greenhouse. The experiment was conducted in 1998, and again in 1999 with minor modifications. In 1998 all replicates were planted in 4 cm pots, and pots from each soil treatment were placed in the same flat and rotated weekly. In 1999 replicates were planted in randomly distributed 6.5 cm pots. There were no significant differences between years so data from 1998 and 1999 were combined; $n = 34$ per treatment combination except for the treatment combination with both high density and sterilized soil where $n = 28$. Data were analysed using backward conditional logistic regression (SPSS, version 6.1.3).

Pathogen isolation

Upon seedling death in field soil, roots were surface sterilized for 5 min in a 5% bleach solution and rinsed in distilled water. Cross-sections from the leading edge of the disease lesion were plated on corn-meal agar. Isolates were subcultured and maintained on corn-meal agar plates. Isolates were identified to genus by Karen Rane, Diagnostic Technician at Purdue Plant and Pest Diagnostic Laboratory, West Lafayette, Indiana. *Pythium* spp. are in the division Oomycota, kingdom Protoctista (not true fungi). Isolates are maintained at Indiana University and available on request. The three most common isolates were used to create inocula grown in a nutrient-rich vermiculite medium. Over 80% of all isolates were one of these three (distinguished on the basis of growth rate; colour and texture were similar). Inoculation treatments are referred to as P1, P2, and P3. To obtain seedlings for screening, ~200 seedlings were collected from an abundant population along a woodland/field margin. Seedlings were within 5 m of each other and in a similar microhabitat, and did not occur beneath a black cherry canopy. Roots were rinsed with distilled water to reduce contamination. Although some seedlings may have been infected when collected, seedlings were randomly distributed among treatments. Plastic pots (6.5 cm) were filled with potting soil and watered. Five millilitres of inoculum were added to a depression created in the centre of each pot. Seedlings were planted into this depression and exposed vermiculite was covered. Two controls were included: potting mix only (control 1); and sterile nutrient-rich medium and potting mix (control 2). There were 40 replicates of each treatment and control. Seedlings were removed upon death. The null hypothesis that survival is independent of treatment was tested using the χ^2 test statistic. Roots from plants dying in each treatment were plated on corn-meal agar to determine whether the fungus could be re-isolated from the roots.

Received 19 November; accepted 22 December 1999.

1. Janzen, D. H. Herbivores and the number of tree species in tropical forests. *Am. Nat.* **104,** 501–508 (1970).
2. Connell, J. H. in *Dynamics in Populations* (eds den Boer, P. J. & Gradwell, G. R.) 298–312 (Center for Agricultural Publishing and Documentation, Wageningen, 1971).
3. Burdon, J. J. *Diseases and Plant Population Biology* (Cambridge Univ. Press, Cambridge, 1987).
4. Florence, R. G. Decline of old-growth forests in relation to some soil microbiological processes. *Ecology* **46,** 52–64 (1965).
5. Bever, J. D., Westover, K. M. & Antonovics, J. Incorporating the soil community into plant population dynamics: the utility of the feedback approach. *J. Ecol.* **85,** 561–573 (1997).
6. Mills, K. E. & Bever, J. D. Maintenance of diversity within plant communities: soil pathogens as agents of negative feedback. *Ecology* **79,** 1595–1601 (1998).
7. Hubbell, S. P. Seed predation and the coexistence of tree species in tropical forests. *Oikos* **35,** 214–229 (1980).
8. Augspurger, C. K. Offspring recruitment around tropical trees: changes in cohort distance with time. *Oikos* **40,** 189–196 (1983).
9. Augspurger, C. K. & Kelly, C. K. Pathogen mortality of tropical tree seedlings: experimental studies of the effects of dispersal distance, seedling density, and light conditions. *Oecologia* **61,** 211–217 (1984).
10. Clark, D. A. & Clark, D. B. Spacing dynamics of a tropical rain forest tree: evaluation of the Janzen–Connell model. *Am. Nat.* **124,** 769–788 (1984).
11. Connell, J. H., Tracey, J. G. & Webb, L. J. Compensatory recruitment, growth and mortality as factors maintaining rain forest tree diversity. *Ecol. Monogr.* **54,** 141–164 (1984).
12. Becker, P., Lee, L. W., Rothman, E. D. & Hamilton, W. D. Seed predation and the coexistence of tree species: Hubbell's models revisited. *Oikos* **44,** 382–390 (1985).
13. Condit, R., Hubbell, S. P. & Foster, R. B. Recruitment of conspecific adults and the maintenance of tree and shrub diversity in a neotropical forest. *Am. Nat.* **140,** 261–286 (1992).
14. Gilbert, G. S., Hubbell, S. P. & Foster, R. B. Density and distance to adult effects of a canker disease of trees in a moist tropical forest. *Oecologia* **98,** 100–108 (1994).
15. Notman, E., Gorchov, D. L. & Cornejo, F. Effect of distance, aggregation, and habitat on levels of seed predation for two mammal-dispersed neotropical rain forest tree species. *Oecologia* **106,** 221–227 (1996).
16. Wills, C., Condit, R., Foster, R. B. & Hubbell, S. P. Strong density- and diversity-related effects help to maintain species diversity in a neotropical forest. *Proc. Natl Acad. Sci.* **94,** 1252–1257 (1997).
17. Schupp, E. W. The Janzen–Connell model for tropical tree diversity: population implications and the importance of spatial scale. *Am. Nat.* **140,** 526–530 (1992).
18. Burkey, T. V. Tropical tree species diversity: A test of the Janzen–Connell model. *Oecologia* **97,** 533–540 (1994).
19. Cintra, R. A test of the Janzen–Connell model with two common tree species in Amazonian forest. *J. Trop. Ecol.* **13,** 641–658 (1997).
20. Burdon, J. J. & Chilvers, G. A. Host density as a factor in plant disease ecology. *Annu. Rev. Phytopathol.* **20,** 143–166 (1982).
21. Fox, J. F. Alternation and coexistence of tree species. *Am. Nat.* **111,** 69–89 (1977).
22. Woods, K. D. Reciprocal replacement and the maintenance of codominance in a beech maple forest. *Oikos* **33,** 31–39 (1979).
23. Van der Putten, W. H. & Peters, B. A. M. How soil-borne pathogens may affect plant competition. *Ecology* **78,** 1785–1795 (1997).
24. Van der Putten, W. H., Van Dijk, C. & Peters, B. A. M. Plant-specific soil-borne diseases contribute to succession in foredune vegetation. *Nature* **362,** 53–56 (1993).
25. Bever, J. D. Feedback between plants and their soil communities in an old field community. *Ecology* **75,** 1965–1977 (1994).
26. Chen, W., Schneider, R. W. & Hoy, J. W. Taxonomic and phylgenetic analyses of ten *Pythium* species using isozyme polymorphisms. *Phytopathology* **82,** 1234–1244 (1992).
27. Carlisle, M. J. & Watkinson, S. C. *The Fungi* (Academic, Harcourt Brace & Co., New York, 1994).
28. Barone, J. A. Host-specificity of folivorous insects in a moist tropical forest. *J. Animal Ecol.* **67,** 400–409 (1998).
29. May, R. M. How many species are there on Earth? *Science* **241,** 1441–1449 (1988).

Acknowledgements

We thank C. Augspurger, G. Gilbert, J. Holah, P. Kover, C. Lively and J. Price for critical review of the manuscript. We also thank R. Wagner for assistance with fungal isolation and identification, and J. Berg, M. Hallinan, M. Hardesty, T. Levitt, A. Overgaard, M. Selby, L. Somers and members of the Clay lab for field assistance. This work was supported by grants to A.P. from the Indiana Academy of Sciences and Indiana University.

Correspondence should be addressed to A.P. (e-mail: apacker@indiana.edu).

The ecological cost of sex

C. Patrick Doncaster*, Graeme E. Pound*† & Simon J. Cox†

* *Division of Biodiversity and Ecology, School of Biological Sciences, University of Southampton, Bassett Crescent East, Southampton SO16 7PX, UK*
† *Department of Electronics and Computer Science, University of Southampton, Highfield, Southampton SO17 1BJ, UK*

Why sex prevails in nature remains one of the great puzzles of evolution[1,2]. Sexual reproduction has an immediate cost relative to asexual reproduction, as males only express their contribution to population growth through females. With no males to sustain, an asexual mutant can double its relative representation in the population in successive generations. This is the widely accepted 'twofold cost of males'[1–3]. Many studies[4–7] have attempted to explain how sex can recoup this cost from fitness benefits associated with the recombination of parental genotypes, but these require complex biological environments that cycle over evolutionary timescales. In contrast, we have considered the ecological dynamics that govern asexual invasion. Here we show the existence of a threshold growth rate for the sexual population, above

which the invasion is halted by intraspecific competition. The asexual population then exerts a weaker inhibitory effect on the carrying capacity of the sexual population than on its own carrying capacity. The stable outcome of this is coexistence on a depleted resource base. Under these ecological circumstances, longer-term benefits of sex may eventually drive out the asexual competitor.

An allele that confers a twofold advantage in growth rate per capita doubles its representation in the population each generation. An asexual species with the same advantage over a sexual species only does so if the population is unbounded by carrying capacity. Here we use a classical ecological model to show this distinction with the fewest possible assumptions. Our model provides a framework for understanding sex and asex as alternative strategies for reproductively isolated sub-populations that compete to consume a common resource. We begin by modelling the dynamics of exploitation competition between two populations of resource consumers. Each has a genetically coded rate constant for conversion of resource uptake into new consumer biomass, and an average lifespan for its members that may be influenced by its environment. We then explore the implications for coexistence if one of these types reproduces sexually and the other invades as an asexual mutant.

Consider a renewing stock of prey exploited to some fraction S of their carrying capacity by a population of predators present at a fraction N of their carrying capacity. Let the predator have a rate of prey consumption per capita that depends directly on prey density. We then represent the dynamics of prey renewal and consumption with a continuous rate equation:

$$\dot{S} = (1 - S)S - NS \tag{1}$$

The first term describes a logistic renewal of prey, from a unitary intrinsic rate to zero at carrying capacity $S = 1$ (in the absence of predation). The second term describes the opposing rate of loss of stock to the predator.

We now distinguish between two species of predator competing to exploit the resource, present at fractions N_1 and N_2 of their respective carrying capacities. Let the rate of consumption by each predator 1 have a component α_{21} accounting for the prey eaten by predator 1 that would otherwise have been eaten by predator 2. In effect, α_{21} describes the consequences to predator 2 of exploitation by predator 1. A matching component α_{12} describes the inhibitory effect of predator 2 on predator 1. If $\alpha_{ij} = 1$, then predator j takes each prey from predator i at the same unitary rate as predator i takes each prey for itself. In this case, the feeding niche of predator j wholly encompasses that of predator i. If $\alpha_{ij} = \alpha_{ji} = 0$, then neither predator uses up any of the prey exploited by the other. In this case, the feeding niches of the predators do not overlap. The conceptual scheme is illustrated in Fig. 1. Two new rate equations then describe the resource available to each species, S_1 and S_2, as fractions of their respective carrying capacities within the niches of N_1 and N_2:

$$\dot{S}_1 = (1 - S_1)S_1 - (N_1 + \alpha_{12}N_2)S_1 \tag{2a}$$

$$\dot{S}_2 = (1 - S_2)S_2 - (N_2 + \alpha_{21}N_1)S_2 \tag{2b}$$

Although these equations describe a single prey species that is shared between two predators, so that S_1 and S_2 are not independent, similar conclusions can be drawn from a model with two independent prey species in which $S_1 + S_2 = S$. Setting the rates of change to zero in equations (2) and solving for S_i yields the equilibrium stock of prey available to each predator species:

$$S_1^* = 1 - (N_1 + \alpha_{12}N_2) \tag{3a}$$

$$S_2^* = 1 - (N_2 + \alpha_{21}N_1) \tag{3b}$$

Finally, consider the dynamics of the two predators. Let each predator i recruit in proportion r_i to its exploitation per capita of S_i prey, and die at a constant rate per capita d_i. Assuming prey renews at relatively fast timescales relative to predator turnover, we can use equations (3) to obtain predator rate equations at prey equilibrium:

$$\dot{N}_1 = r_1[1 - (N_1 + \alpha_{12}N_2)]N_1 - d_1N_1 \tag{4a}$$

$$\dot{N}_2 = r_2[1 - (N_2 + \alpha_{21}N_1)]N_2 - d_2N_2 \tag{4b}$$

Equations (4) describe a logistic recruitment of predator i for a given N_j, from an intrinsic rate per capita r_i to zero at the maximum density of 1 in the absence of losses d_i. This is the classical Lotka–Volterra model of interspecific competition[8,9]. Crucially, for the purposes of our argument, we have expanded it to allow for separate components of mortality d_i and therefore separate birth and death processes, rather than combining them in the conventional net growth rate. Each predator has a steady-state abundance given by setting its rate equation to zero and solving for N_i:

$$N_1^* = k_1 - \alpha_{12}N_2, \text{ where } k_1 = 1 - \frac{d_1}{r_1} \tag{5a}$$

$$N_2^* = k_2 - \alpha_{21}N_1, \text{ where } k_2 = 1 - \frac{d_2}{r_2} \tag{5b}$$

The constant k_i is the carrying capacity of predator i in the absence of the other consumer. The equilibrium abundance of each thus depends on the abundance of the other. By plotting these zero isoclines on the phase plane of N_1 and N_2, we can explore the parameter values that allow coexistence of the two predators. In fact, coexistence requires that $k_1/\alpha_{12} > k_2$ and $k_2/\alpha_{21} > k_1$, as illustrated by the example in Fig. 2a. This yields a stable equilibrium of positive (N_1^*, N_2^*) at the intersection of the isoclines, towards which any positive (N_1, N_2) converges. In biological terms, this means that each predator must have a smaller competitive effect on the carrying capacity of the other than it has on its own carrying capacity through intraspecific competition. Any other arrangement of isoclines produces extinction of one or the other predator[10]. If predator j exerts a stronger inhibitory effect on the carrying capacity of predator i than it exerts on its own carrying capacity ($k_i/\alpha_{ij} < k_j$), then predator j will replace predator i.

We now consider the particular case of a sexually reproducing

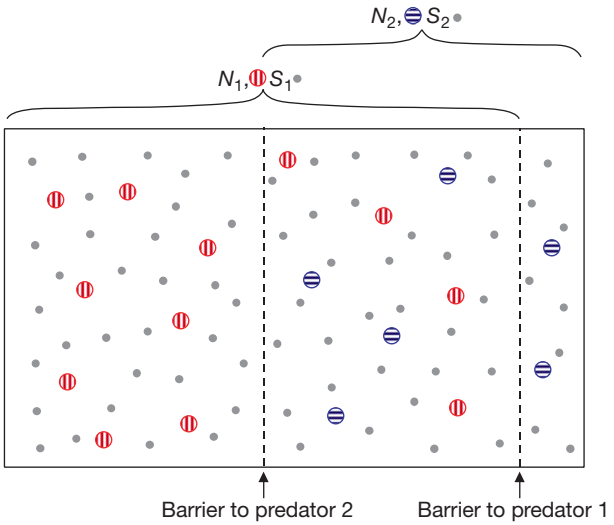

Figure 1 Conceptual scheme for exploitation by a predator 1 (red vertical stripe) and a predator 2 (blue horizontal stripe) of a renewing stock of limiting prey (grey filled dots). Coexistence is possible if the two resource niches are not identical, otherwise the species with the faster potential for population growth (given by r_i/d_i) outcompetes the other at equilibrium resource use, following Gause's competitive exclusion principle. In this example, only the middle section of the arena is exploited by both species ($\alpha_{12} = 0.5$, $\alpha_{21} = 0.8$).

anisogamous predator 1 that produces an asexual mutant predator 2. The cost of males gives predator 1 an intrinsic growth rate per capita half that of predator 2 on average, so $r_1 = 0.5r_2$. This means that we assume an identical intrinsic birth rate per capita for asexual individuals and sexual females, and zero birth rate for males which constitute half the sexual population. If the two types differ only in this respect, we can expect $d_1 = d_2$. It is then useful to define $R_0 = r_1/d_1$, which describes the capacity for growth of the sexual population. R_0 refers to the average number of offspring born to each sexual individual before it dies, in the absence of both intra- and interspecific competition (the subscript zero referring to the sexual population at time zero when the first consumer converts prey into offspring). The carrying capacities now become:

$$k_1 = 1 - \frac{1}{R_0} \text{ and } k_2 = 1 - \frac{1}{2R_0} \quad (6)$$

The twofold difference in growth capacity yields a larger carrying capacity for predator 2 than predator 1, reflecting its greater efficiency of converting food into new predator biomass. This is accommodated by a reduction in equilibrium prey stock. Figure 2b shows the sequence of events as an asexual mutant invades a sexual population. The larger carrying capacity of the asexuals contributes to their higher equilibrium presence, at the expense of the sexuals. Crucially, however, the twofold greater growth capacity of the asexuals has an influence on the dynamics of asexual invasion that depends on the absolute size of R_0. Larger values of R_0 reduce the difference between k_2 and k_1 (equations (6)), and therefore between N_2^* and N_1^* (equations (5)). If R_0 is substantially greater than unity, the twofold cost of males will have little consequence on the dynamics of an asexual invasion. Figure 3 shows how sexuals and asexuals reach an asymptotic ratio as R_0 becomes infinitely large. Both types then have an infinite lifespan ($d_1 = d_2 = 0$), which means that their equilibrium populations have zero birth rates and the asexuals are thus unable to realize their superior growth capacity. The ratio of sexuals to asexuals diminishes as R_0 approaches unity. Sexuals cannot persist with asexuals below a threshold R_0, defined by the twofold difference in reproductive capacity and the competition coefficient of the asexual α_{12} (Fig. 3). Figure 4 shows how a high growth capacity permits coexistence even with a high competitive impact of asexuals on sexuals (α_{12} approaching 1), and that coexistence at lower R_0 requires a correspondingly lower minimum α_{12}.

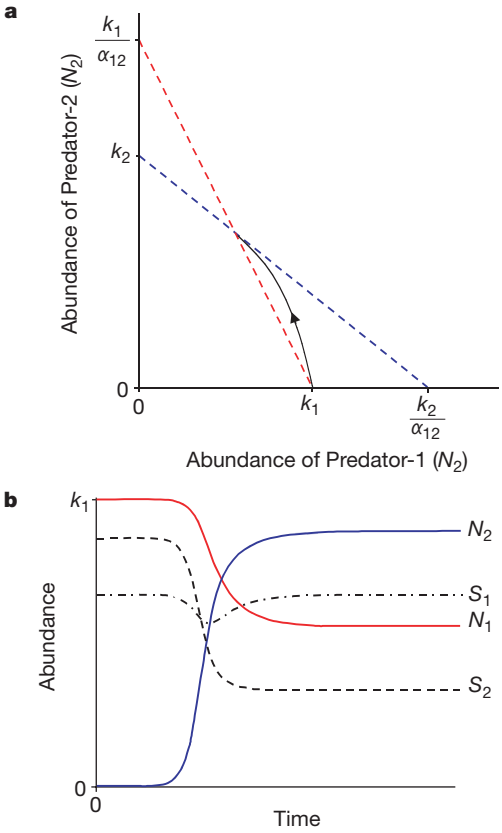

Figure 2 Population dynamics of exploitation competition. **a**, Phase plane for two species of competing consumers. The steeper of the two broken lines is the isocline for exploitation by predator 1 at a given abundance of predator 2, and the other is the isocline for exploitation by predator 2 at a given abundance of predator 1 (equations (5)). The example shows stable coexistence at the intersection of the isoclines when a sexual predator 1 is invaded by an asexual predator 2 with twice the capacity for growth (arrow). $\alpha_{12} = 0.5$, $\alpha_{21} = 0.8$, $r_1 = 0.5r_2$, $d_1 = d_2 = 0.04$, $R_0 = 2.5$ (predator 1). At $t = 0$, $N_1 = k_1$, $N_2 = 0.0001$. Abundance and time are non-dimensionalized. **b**, Re-equilibration over time of example in **a**. Each predator i uses resource S_i, and $\dot{N}_i = r_i S_i N_i - d_i N_i$, with $\dot{S}_i$ given by equations (2).

Provided that $k_1/k_2 > \alpha_{12}$, the sexual population coexists with the asexual invaders, or even drives them out altogether if $k_1 > k_2/\alpha_{21}$ (Fig. 2a). We assume that the sexual predator 1 has less impact on the growth of the asexual predator 2 than the asexual has on its own growth, so $\alpha_{21} < 1$. This is because the self-identical asexual individuals (barring further mutations) must experience the strongest possible intraspecific competition. We further propose that the asexual predator 2 is likely to have less impact on the sexual predator 1 than the sexual has on its own growth, even at the very start of the invasion, so $\alpha_{12} < 1$. This is reasonable if the asexual mutant has been cloned from one or a few sexual genotypes, so that its population represents only a small sample of the genetic pool to which the sexual population belongs[11]. This type of founder effect restricts the asexual to a narrower niche than is occupied by the sexual, given genetic variability for resource exploitation in the sexual population[12]. Recent examples of resource partitioning between clones support a relationship between environmental heterogeneity and genetic variation[13–16]. Empirical evidence that differences in niche breadth may explain coexistence of sexual and asexual populations has been found for several species, including the freshwater snail *Potamopyrgus*[17], the fish *Poeciliopsis*[18] and the lizard *Cnemidophorus*[19]. In the longer term, character displacement in the sexual predator 1 and mutation and selection in the asexual predator 2 seem likely to further reduce the value of α_{12}. In the event that $d_1 < d_2$ such that $k_1 > k_2$, the sexual type persists even with $\alpha_{12} = 1$. Disruptive selection is likely to cause d_1 to change with respect to d_2, particularly in the form of character displacement by the genetically variable sexuals as a result of competition with the self-identical asexuals[20].

Although the cost of males is clearly ecology dependent, it remains widely cited as a twofold disadvantage that must be

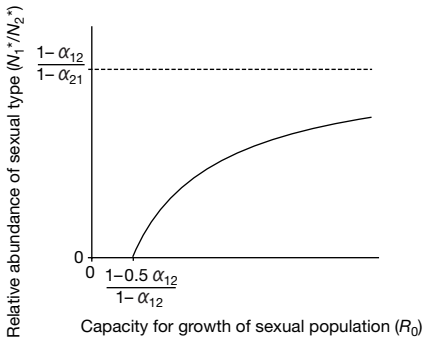

Figure 3 Influence of the growth capacity of sexual predator 1 ($R_0 = r_1/d_1$) on the equilibrium ratio of sexuals of asexuals. As in Fig. 2, $r_1 = 0.5r_2$, $d_1 = d_2 = 0.04$. The relative abundance of sexuals has an asymptote for large R_0, given by the dotted line. Smaller values of α_{12} increase this asymptote, and decrease the threshold R_0 for coexistence. Unless $\alpha_{12} \geq 1$, there always exists some R_0 that will support a sexual population.

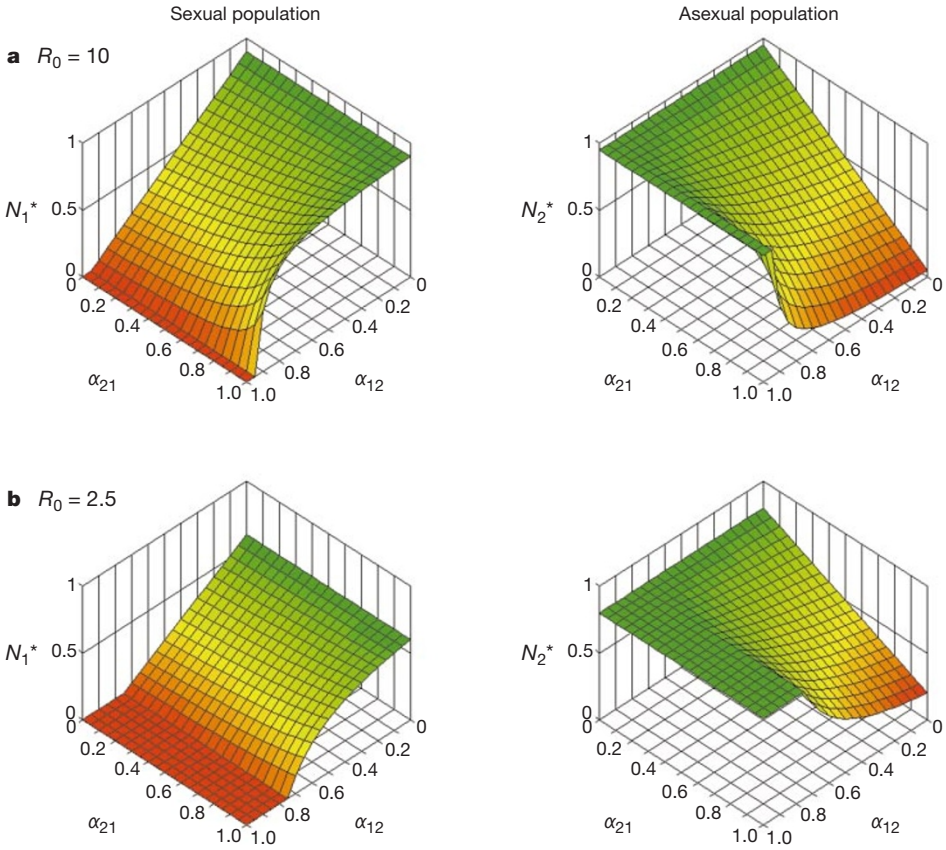

Figure 4 Influence of competition coefficients α_{12} and α_{21} on equilibrium densities of sexual and asexual populations. **a**, Sexual population with a high capacity for growth, $R_0 = 10$, given by $d_1 = 0.01$. **b**, Sexual population with a lower capacity for growth, $R_0 = 2.5$ as Fig. 2, given by $d_1 = 0.04$; other parameter values as in Figs 1–3.

recouped in adaptive payoffs from the recombination of parental genotypes[2,21–25]. Why do evolutionary biologists continue to ignore the evidence from population ecology? We note from the literature that ecological outcomes have previously been proposed with the aid of purpose-built models rather than drawing on the standard framework of Lotka–Volterra competition equations, with some loss of generality in consequence. A pioneering study by Case and Taper[26] sought conditions for coexistence from a more elaborate treatment incorporating marriage functions and resource-dependent death rates. They had dismissed the classical Lotka–Volterra model as unrepresentative of competition between sexual and asexual types, on the grounds that it failed to separate birth and death processes in the predator dynamics. Indeed, the usual quotations of equations (4) in the literature omit explicit parameters d_i, so as to express predator recruitment in terms of net growth rates[10]. As such, they give a steady-state growth of zero by definition and so differences in fecundity cannot influence equilibrium coexistence. This does not invalidate the rationale of the Lotka–Volterra model. Our use of separate birth and death terms has revealed the key parameters R_0 and α_{12} that control the ecological impact of male presence on the outcome of competition with asexual mutants. Our conceptual scheme shown in Fig. 1 furthermore indicates that the outcome of competition between populations of consumers may also apply to distributions of species occupying a habitat. If the resource points shown in Fig. 1 are occupied rather than eaten, at a rate r_i, and renew upon local extinction of the colonist at a rate d_i, then our rate equations (4) apply to the well-known Levins model[27] of metapopulation dynamics[28].

Our application of classical population dynamics has shown how intraspecific competition can halt the invasion of an asexual mutant into a sexual population (Fig. 2). Coexistence is immediately possible if the invading asexuals have a smaller inhibitory effect on the exploitative abilities of the sexuals than the sexuals have on themselves. The coefficient describing this relative effect, α_{12}, governs a threshold for the growth capacity of the sexual population, below which sexuals cannot compete with the asexual invaders (Fig. 3). Above this threshold, it is self-regulation of asexuals through intraspecific competition that halts their population growth before extinction of the sexual population. We therefore conclude that the twofold cost of males to the growth capacity of the sexual population does not automatically pose a threat to the survival of the sexual strategy. Males are less costly to species with high growth capacities. Strong intraspecific competition favours coexistence after an asexual invasion, giving the sexual strategy more time than was previously thought[29] in which to express its well known evolutionary advantages over asex. □

Received 9 November 1999; accepted 24 January 2000.

1. Williams, G. C. *Sex and Evolution* (Princeton Univ. Press, Princeton, 1975).
2. Ridley, M. *Evolution* 2nd edn (Blackwell Science, Oxford, 1996).
3. Maynard Smith, J. *The Evolution of Sex* (Cambridge Univ. Press, Cambridge, UK, 1978).
4. Kondrashov, A. S. Classification of hypotheses on the advantage of amphimixis. *J. Hered.* **84,** 372–387 (1993).
5. Judson, O. P. & Normark, B. B. Ancient asexual scandals. *Trends Ecol. Evol.* **11,** 41–46 (1996).
6. Hurst, L. D. & Peck, J. R. Recent advances in understanding of the evolution and maintenance of sex. *Trends Ecol. Evol.* **11,** 46–52 (1996).
7. Hamilton, W. D., Axelrod, R. & Tanese, R. Sexual reproduction as an adaptation to resist parasites. *Proc. Natl Acad. Sci. USA* **87,** 3566–3573 (1990).
8. Volterra, V. in *Animal Ecology* (ed. Chapman, R. N.) 409–448 (McGraw Hill, New York, 1931).
9. Lotka, A. J. The growth of mixed populations: two species competing for a common food supply. *J. Wash. Acad. Sci.* **22,** 461–469 (1932).
10. Begon, M., Harper, J. L. & Townsend, C. R. *Ecology* 3rd edn (Blackwell Science, Oxford, 1996).
11. Vrijenhoek, R. C. Factors affecting clonal diversity and coexistence. *Am. Zool.* **19,** 787–797 (1979).
12. Bell, G. *The Masterpiece of Nature* (Croom Helm, London, 1982).
13. Browne, R. A. & Hoopes, C. W. Genotype diversity and selection in asexual brine shrimp (*Artemia*). *Evolution* **44,** 1035–1051 (1990).
14. Bolger, D. T. & Case, T. J. Divergent ecology of sympatric clones of the asexual gecko, *Lepidodactylus lugubris*. *Oecologia* **100,** 397–405 (1994).

15. Semlitsch, R. D., Hotz, H. & Guex, G. D. Competition among tadpoles of coexisting hemiclones of hybridogenetic *Rana esculenta*: support for the frozen niche variation model. *Evolution* **51,** 1249–1261 (1997).
16. Weeks, A. R. & Hoffmann, A. A. Intense selection of mite clones in a heterogeneous environment. *Evolution* **52,** 1325–1333 (1998).
17. Jokela, J., Lively, C. M., Fox, J. A. & Dybdahl, M. F. Flat reaction norms and "frozen" phenotypic variation in clonal snails (*Potamopyrgus antipodarum*). *Evolution* **51,** 1120–1129 (1997).
18. Vjijenhoek, R. C. & Pfeiler, E. Differential survival of sexual and asexual *Poeciliopsis* during environmental stress. *Evolution* **51,** 1593–1600 (1997).
19. Case, T. J. Patterns of coexistence in sexual and asexual species of *Cnemidophorus* lizards. *Oecologia* **83,** 220–227 (1990).
20. Doebeli, M. An explicit genetic model for ecological character displacement. *Ecology* **77,** 510–520 (1996).
21. Skelton, P. (ed.) *Evolution: a Biological and Palaeontological Approach* (Addison-Wesley, Wokingham, UK, 1993).
22. Bulmer, M. *Theoretical Evolutionary Ecology* (Sinauer, Sunderland, Massachusetts, 1994).
23. Futuyma, D. J. *Evolutionary Biology* 3rd edn (Sinauer, Sunderland, Massachusetts, 1998).
24. Maynard Smith, J. *Evolutionary Genetics* 2nd edn (Oxford Univ. Press, Oxford, 1998).
25. Stearns, S. C. & Hoekstra, R. F. *Evolution: an Introduction* (Oxford Univ. Press, Oxford, 2000).
26. Case, T. J. & Taper, M. L. On the coexistence and coevolution of asexual and sexual competitors. *Evolution* **40,** 366–387 (1986).
27. Levins, R. in *Lectures on Mathematics in the Life Sciences, vol. 2* (ed. Gerstenhaber, M.) 75–107 (American Mathematical Society, Providence, 1970).
28. Connolly, S. R. & Roughgarden, J. Theory of marine communities: competition, predation, and recruitment-dependent interaction strength. *Ecol. Monogr.* **69,** 277–296 (1999).
29. Lively, C. M. Host-parasite coevolution and sex. *BioScience* **46,** 107–114 (1996).

Acknowledgements

We thank G. F. Turner, S. J. Hawkins and C. P. Please for clarifications of key issues. This work was supported by a Natural Environment Research Council grant to C.P.D., and by an Engineering and Physical Sciences Research Council studentship to G.E.P.

Correspondence should be addressed to C.P.D. (e-mail: cpd@soton.ac.uk).

NMDA spikes in basal dendrites of cortical pyramidal neurons

Jackie Schiller*, Guy Major†‡, Helmut J. Koester‡§ & Yitzhak Schiller‡‖

* *Departments of Physiology and Biophysics, Technion Medical School, Bat-Galim, Haifa 31096, Israel*
† *Biological Computation Research-Bell Laboratories, Lucent Technologies, 600 Mountain Avenue, Murray Hill, New Jersey, USA and University Laboratory of Physiology, Oxford, UK*
§ *Department of Cell Physiology, Max-Planck-Institute for Medical Research, Heidelberg, Germany*
‖ *Department of Neurology, Rambam Medical Center, Haifa, Israel*
‡ *These authors contributed equally to this work*

Basal dendrites are a major target for synaptic inputs innervating cortical pyramidal neurons[1]. At present little is known about signal processing in these fine dendrites. Here we show that co-activation of clustered neighbouring basal inputs initiated local dendritic spikes, which resulted in a 5.9 ± 1.5 mV (peak) and 64.4 ± 19.8 ms (half-width) cable-filtered voltage change at the soma that amplified the somatic voltage response by 226 ± 46%. These spikes were accompanied by large calcium transients restricted to the activated dendritic segment. In contrast to conventional sodium or calcium spikes, these spikes were mediated mostly by NMDA (*N*-methyl-D-aspartate) receptor channels, which contributed at least 80% of the total charge. The ionic mechanism of these NMDA spikes may allow 'dynamic spike-initiation zones', set by the spatial distribution of glutamate pre-bound to NMDA receptors, which in turn would depend on recent and ongoing activity in the cortical network. In addition, NMDA spikes may serve as a powerful mechanism for modification of the cortical network by inducing long-term strengthening of co-activated neighbouring inputs.

To explore synaptic processing in basal dendrites we identified fine dendritic branches using fluorescence confocal microscopy and mimicked excitatory postsynaptic potentials (EPSPs) by ultraviolet laser glutamate uncaging. Figure 1a compares a synaptically evoked EPSP with an excitatory postsynaptic-like potential (EPSLP) evoked by a 1-ms ultraviolet laser pulse directed to a basal dendrite in the presence of 1 mM extracellular caged glutamate. The two post-synaptic potentials were similar except that EPSLPs were slower and had a larger NMDA component (see Methods for details).

Figure 1b shows EPSLPs evoked in a distal basal dendrite at various laser intensities. At a certain threshold intensity, a small increase in the laser intensity more than doubled the EPSLP amplitude recorded at the soma (Fig. 1b). Beyond that threshold intensity only a small additional increase in EPSLP peak amplitude occurred when the laser power was increased (Fig. 1b, $n = 14$ cells). The threshold and all-or-none nature of the response indicated initiation of local dendritic spikes. The mean amplitude of just subthreshold cable-filtered responses was 3.9 ± 1.1 mV, and the amplitude of the cable-filtered basal dendritic spike was 5.2 ± 1.7 mV, as measured at the soma ($n = 14$). Unless otherwise specified, the terms 'suprathreshold' and 'subthreshold' are taken to mean 'suprathreshold in the dendrite' and 'subthreshold in the dendrite', respectively. All EPSLPs presented were subthreshold with respect to axonal action potentials. Hyperpolarization of the membrane potential reduced the amplitudes of the suprathreshold EPSLPs to subthreshold levels (Fig. 1c, $n = 4$). Calcium imaging revealed that suprathreshold EPSLPs evoked a large localized increase in calcium influx limited to a roughly 20-μm stretch of the activated basal dendrite (Fig. 1d, $n = 5$). These observations are consistent with initiation of a local spike by focal glutamate uncaging onto a single basal dendrite.

Subthreshold EPSLPs were not affected by addition of either the specific voltage-gated sodium channel (VGSC) blocker tetrodotoxin (TTX; 1 μM) (96 ± 10% of control value, $n = 7$) or the voltage-gated calcium channel (VGCC) blocker cadmium (50–150 μM) (95 ± 6% of control value, $n = 10$). In contrast, TTX and cadmium substantially reduced the amplitudes and time integrals of supra-threshold EPSLPs (Fig. 2a, b). The average threshold for basal dendritic spike initiation measured at the soma was 4.2 ± 1.4 mV ($n = 7$) for TTX and 4.4 ± 1.8 mV ($n = 10$) for cadmium. The sodium and calcium-dependent cable-filtered spikes added 5.0 ± 2.1 mV (half-width of 60 ± 16 ms) and 4.7 ± 1.8 mV (half-width of 58 ± 15 ms) to the somatic potential, respectively.

Basal dendritic spikes could be reinitiated following blockade of either VGSCs or VGCCs. The threshold laser intensity for spike initiation increased by 29 ± 6% in the presence of TTX and 101 ± 9% in the presence of cadmium. The reinitiated spikes were similar to the original spikes evoked under control conditions (Fig. 2c). The averaged peak and time integral of the reinitiated spikes were 95.7 ± 8.2% and 117.3 ± 33.5% of the original spikes ($n = 6$). These results indicated that although VGCCs and VGSCs participated in the initiation of the basal dendritic spike, a third dendritic conductance probably served as the major charge carrier. Furthermore, the fact that basal dendritic spikes could be reinitiated in the presence of either TTX or cadmium ruled out the possibility that these spikes resulted from a polysynaptic or circuit effect.

When glutamate was uncaged at the soma, there were no sudden jumps in response amplitude as laser intensity was increased. Furthermore, TTX and cadmium did not noticeably change somatic EPSLPs (101 ± 11% and 104 ± 4% of control, $n = 6$ and 7, respectively). Thus, somatic VGSCs and VGCCs did not contribute to basal dendritic spikes.

Initiation of local basal dendritic spikes was limited to distal basal dendrites (>70 μm away from the soma). In three neurons the difference between the distal and proximal dendrite was observed for the same basal dendrite.

Basal dendritic spikes were critically dependent on activation of